Hindawi
Advances in Materials Science and Engineering
Volume 2024, Article ID 2395548, 18 pages
https://doi.org/10.1155/2024/2395548

Research Article

Testing and Evaluation of Hard Sandstone Aggregate in Hot Mix Asphalt

Liu PeiRong,[1,2] **Yang LiMing**,[3] **Huang Jun**,[1] **Li ChaoYang**,[1] **and Yang DaTian**[4]

[1]*Guanxi Liubin Expressway Construction & Development Co., Ltd., Nanning 530023, China*
[2]*Guanxi Nanning Second Ring Expressway Co., Ltd., Nanning 530029, China*
[3]*Guangxi Communication Design Group Co., Ltd., Nanning 530029, China*
[4]*College of Civil Engineering, Chongqing Jiaotong University, Chongqing 400074, China*

Correspondence should be addressed to Yang DaTian; tywoyangda@cqjtu.edu.cn

Received 2 January 2024; Revised 2 April 2024; Accepted 9 April 2024; Published 14 May 2024

Academic Editor: Yuri Ribakov

To address the shortage of the aggregate used in a hot mix asphalt (HMA) pavement in Guangxi, properties such as the aggregate crushing, polished stone, and Los Angeles abrasion values of a type of hard sandstone aggregate used in HMA were tested after various conditioning treatments. The hard sandstone aggregate met the technical requirements for aggregate in HMA. In addition, the influence of the Marshall compaction on the hard sandstone aggregate-combined grading was tested. The combined grading curve changed a little, and the aggregate satisfied the corresponding technical requirements. Therefore, according to the abovementioned results, the hard sandstone aggregate can be used as a coarse aggregate in HMA.

1. Introduction

In recent decades, with the continuous demand for a high-quality asphalt pavement, there has been an increasing shortage of aggregates, such as basalt and dolerite, for use in asphalt mixtures, and as a result, their prices have risen. To increase the availability of aggregates for use in asphalt mixtures, a type of hard sandstone aggregate was introduced. Ouyang et al. [1] used sandstone aggregates in asphalt mixtures, studied their performance in highways, and indicated that these aggregates could be used in asphalt. Metcalf and Goetz [2] also found that sandstone aggregates could be used in the asphalt pavement. Hunsucker and Graves [3] found that the hot mix asphalt (HMA)-used sandstone aggregate is resistant to rutting and that the application of an asphalt sandstone base and surface mixtures has been very successful.

Zhang and Li [4] used the sandstone aggregate to produce sandstone concrete as a road base. Li et al. [5] studied the feasibility of replacing limestone aggregates with sandstone aggregates. Yılmaz and Tugrul [6] studied the effects of different sandstones on the concrete strength and found that concrete mixtures made of subarkose aggregates had approximately 40–50% greater compressive and splitting tensile strengths than those made of subarkose-arkose, sublitharenite-litharenite, and arkose aggregates. Yang et al. [7] studied the mechanical properties and durability of concrete made from sandstone aggregates.

It can be seen from the abovementioned literature that sandstone has been primarily used for cement concrete and less used for the HMA pavement. In contrast, limestone, diabase, basalt, and broken gravel have been extensively used in HMA. Their properties are listed in Table 1.

Shi et al. found that the crushing value of aggregates increased as the temperature increased [12].

During the process of mixing, paving, and rolling HMA, the aggregates are consistently maintained at high temperatures (approximately 130–200°C). When the HMA pavement is subjected to high- and low-temperature cycles, the aggregates in HMA go through the same cycle of high and low temperatures. Aggregates may be crushed by the paver and rollers during the paving and rolling process, so the aggregate gradation will change. Hence, the properties of aggregates, such as the crushing value, polished stone value

Table 1: Properties of limestone, diabase, basalt, and gravel aggregate [8–11].

Test item	Limestone	Basalt	Diabase	Gravel
Apparent relative density	2.674–2.892	2.724–3.020	2.48–2.983	2.842
Crushing value (%)	12.7–22.2	9.1–12.9	12.2–12.4	10.1
Polishing value (%)	40.2–43	42–47.1	45–49.3	44
Los Angeles abrasion loss (%)	13.6–17.7	5.8–13.6	6.8–14.1	13.5
Water absorption	0.43–0.52	1.08–1.02	—	—

(PSV), and Los Angeles abrasion loss, must be tested before and after conditioning since they influence the long-term performance of the HMA pavement.

In order to apply hard sandstone aggregates widely and solve the aggregate shortage problem for HMA, their properties were tested before and after conditioning in this study. The testing process was as follows. First, the properties of the hard sandstone aggregate were tested using the standard method. Second, the crushing values were measured after the hard sandstone aggregate was heated, dried, and went through freeze-thaw cycles. Third, the polished stone and Los Angeles abrasion values were measured after the hard sandstone aggregate went through the freeze-thaw cycles. Fourth, the surface energy of the hard sandstone aggregate was measured with the capillary rise method (CRM) and compared with those of other types of aggregates. To assess the effect of paving and rolling on the combined aggregate gradation, simulations were performed using a Marshall compactor. The moisture susceptibility of HMA containing the hard sandstone aggregate was evaluated by the indirect tensile strength ratio (TSR) and the modulus ratio (MR), and the polishing tests of HMA were conducted with a three-wheel polishing tester. Figure 1 illustrates the flowchart of the work performed in this study.

2. Testing Method and Aggregate Conditioning

2.1. Testing Method

2.1.1. Sampling Methodology. The hard sandstone aggregate came from a pile of an aggregate plant's pile yard. We first removed the unrepresentative part of the pile foot and then obtained a group of roughly equal parts from several different parts evenly distributed on the top, middle, and bottom of the pile. The sample was representative of the condition and quality of the lot.

To obtain a representative sample, the quartering method was applied. The aggregate was placed on a plate, mixed evenly in the natural state, roughly flattened, and then spread out from the center to the side in two perpendicular directions. The sample was then divided into roughly four equal parts and two parts of the diagonal were remixed. The abovementioned process was repeated until the amount of the material after the reduction was slightly greater than the amount necessary for the tests.

2.1.2. Aggregate Crushing Test. The aggregate crushing value of the coarse aggregate is the relative resistance of the aggregate to crushing under a gradually applied compressive load. First, coarse aggregates with particle sizes of 9.5–13.2 mm were selected after being dried in an oven. Second, the amount of coarse aggregates required for testing was added in three layers to a cylinder that was 11.5 cm in diameter and 18 cm in height, where each layer was subjected to 25 strokes with a tamping rod. Third, the surface of the aggregate sample in the container was carefully leveled, and a plunger was inserted. A total load of 400 kN was applied in 10 min. Finally, the sample was sorted with a 2.36 mm sieve, and the fraction passing through the sieve was weighed. The aggregate crushing value was the percentage of the weight of particles with diameters less than 2.36 mm to the weight of the total sample.

2.1.3. Los Angeles Abrasion Test. First, the sample was prepared and placed in an abrasion test machine. Second, a specified number of steel spheres were then placed in the machine, and the drum was rotated for 500 revolutions at a speed of 30–33 rpm. The sample was then sorted with a 1.70 mm sieve, and the aggregates larger than 1.7 mm were retained on a 1.70 mm (no. 12) sieve, washed with water, and dried in an oven. The percentage loss was obtained by calculating the relative difference between the retained material (larger particles) weight and the original sample weight.

2.1.4. Polished Stone Test. Four curved test specimens were prepared from each sample undergoing testing. Fourteen specimens were clamped around the periphery of a rubber "road wheel" and subjected to two phases of polishing by the rubber wheel. The first phase was abrasion by #30 coarse diamond sand for 3 h, followed by 3 h of polishing with #280 fine diamond sand. Two of the 14 samples were control specimens. The PSV of the hard sandstone coarse aggregate was then measured using a portable skid resistance tester with a special narrow slide.

2.1.5. Surface Free Energy Test. The surface free energy of the hard sandstone aggregate was measured using the CRM. The CRM was described in detail by Dennis Sinkonde et al. [15].

2.1.6. Marshall Compaction. Road rollers can crush the aggregate during compaction of an asphalt mixture, which would change the combined aggregate grading of the asphalt mixture. Hence, in the laboratory, the hard sandstone AC-13C with an asphalt-aggregate ratio of 4.6% was compacted with 75 blows on both sides using a Marshall compactor.

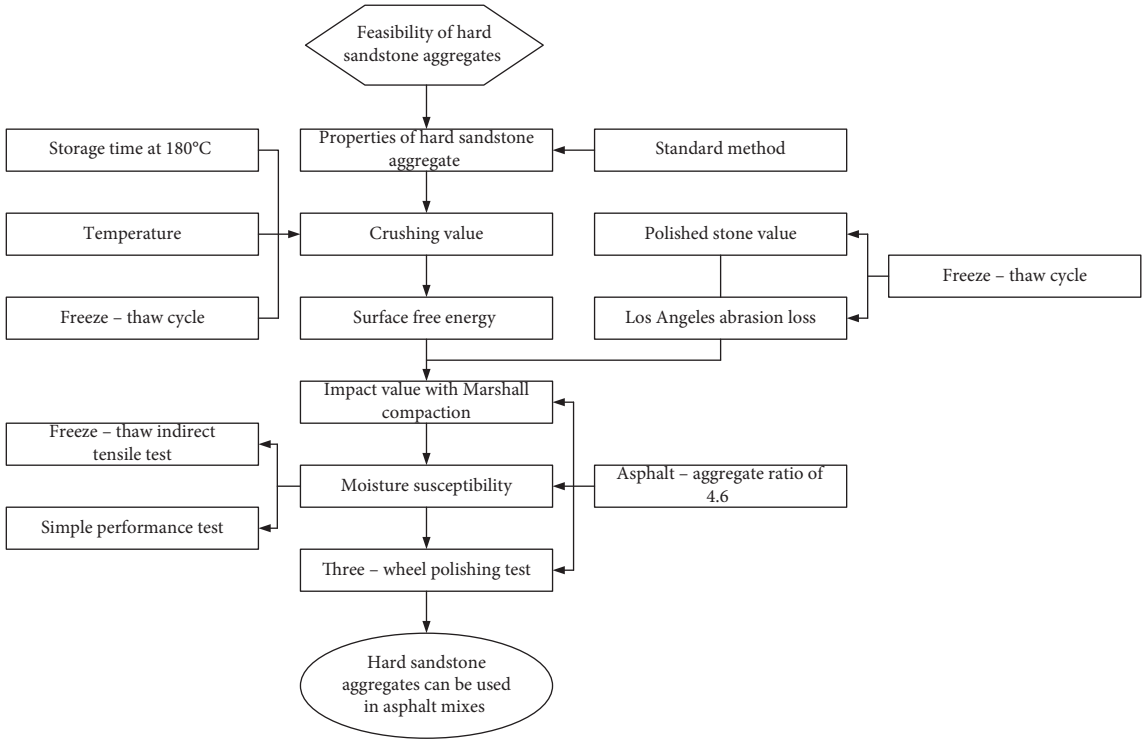

Figure 1: Study flowchart.

2.1.7. Indirect Tensile Ratio Method. Two groups of standard Marshall specimens were formed by double-sided compaction 50 times, with six specimens in each group. One group of specimens was followed by saturation of the sample by applying a vacuum of 730–740 mm Hg for 15 minutes and placed in a plastic bag containing 10 ± 0.5 ml of water and sealed. The specimens were frozen at $-18 \pm 2^{\circ}$C for 16 ± 1 h and then boiled in $60 \pm 0.5^{\circ}$C water for 24 h. The two groups of specimens were kept in water at $25 \pm 0.5^{\circ}$C for no less than 2 h, and the maximum load was obtained at the speed of 50 mm per minute for the two groups of specimens. The indirect tensile strengths (S_t, kPa) of the two groups were calculated as follows:

$$S_t = \frac{2000P}{\pi t D}, \tag{1}$$

where P is the maximum load (N), t is the specimen height immediately before the test (mm), and D is the specimen diameter (mm). The indirect *TSR* was calculated as follows:

$$\text{TSR} = \frac{S_2}{S_1}, \tag{2}$$

where S_2 is the average tensile strength of the moisture-conditioned groups, and S_1 is the average tensile strength of the dry groups.

2.1.8. Simple Performance Test. Six cylindrical specimens with diameters of 150 mm and heights of 155 mm were formed with a rotary compacting instrument, with three in each group, and the void ratio was 7%. Specimens with diameters of 100 mm were drilled with a core drilling machine and then cut to lengths of 150 mm with a cutting machine. One group was followed by saturation of the sample by applying a vacuum of 730–740 mm Hg for 15 minutes and placed in a plastic bag containing 10 ± 0.5 ml of water and sealed. The specimens were frozen at $-18 \pm 2^{\circ}$C for 16 ± 1 h and then boiled in $60 \pm 0.5^{\circ}$C water for 24 h. The simple performance was measured on a simple performance tester at temperatures of 5°C, 20°C, and 40°C and frequencies of 0.01, 0.1, 1, and 10 Hz, as shown in Figure 2.

The *MR* was calculated as follows:

$$MR = \frac{M_2}{M_1}, \tag{3}$$

where M_2 is the average dynamic modulus of the moisture-conditioned groups, and M_1 is the average dynamic modulus of the dry groups.

2.1.9. Three-Wheel Polishing Test. The three-wheel polishing tester consisted of various components, including three tires, weights, turning devices, water spraying devices, and control devices, as shown in Figure 3. The loading speed was 75 times per minute. The load size and the tire shape and type could be varied. The tire rotation diameter was 300 mm.

The water-spraying device could wash off the particles, simulating wet environment conditions and also prolonging the service life of the tire. Water mainly reduces the surface temperature of the tire and reduces tire softening. In previous studies [25, 26], it has been observed that inflatable rubber tires are susceptible to wear and rupture in practical applications. To enhance the efficiency of the aggregate polishing process, we opted for a polyester tire measuring

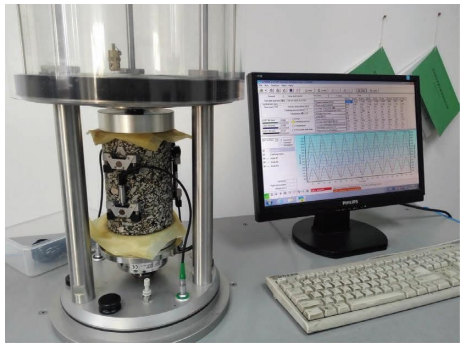

Figure 2: Simple performance test.

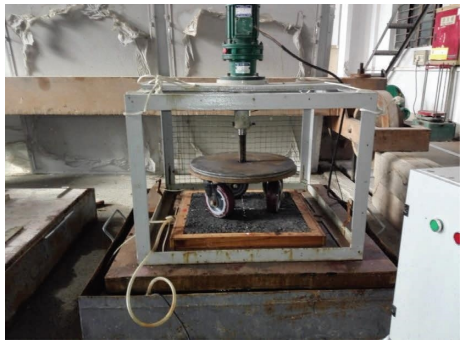

Figure 3: Three-wheel polishing tester.

150 mm in diameter and 50 mm in width, possessing a Shore hardness of 85 [27]. A counterweight of approximately 46.9 kg was used, as depicted in Figure 4.

The wheel track width generated during this test fell within the range of 30–35 mm. To test the tilting friction coefficient, a rubber sheet with dimensions of 37.75 mm × 25.4 mm × 6.35 mm was used, as depicted in Figure 5. When employing the rubber sheet size in the pendulum friction coefficient tester, the reading of the pendulum friction coefficient was observed within the range of 0–1.0 or 0–100 (beyond the scale line), as shown in Figure 6. According to the division in Figure 7, the British pendulum numbers at four locations were used to observe the friction variation characteristics of the hard sandstone asphalt mixture in the accelerated loading test using the three-wheel polishing tester.

2.2. Hard Sandstone Aggregate Conditioning

2.2.1. Heated and Dried Using Natural Gas Combustion and Stored in an Oven at 180°C

(1) In the laboratory, the hard sandstone aggregate samples were first heated and dried using natural gas combustion for 30 min to simulate the process of the aggregate being heated and dried by fuel in a drying drum, as shown in Figure 8.

(2) After the hard sandstone aggregate samples were heated and dried, they were stored in the electric blast drying oven to simulate the storage of aggregate in hot bins. After they were stored for 30, 60, and 120 min in the electric blast drying oven at 180°C, their crushing values were measured at 180°C.

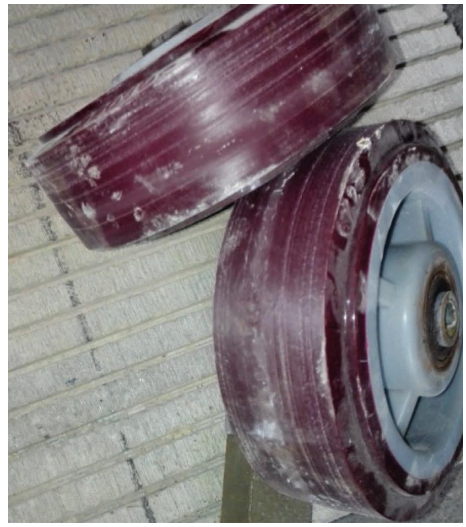

Figure 4: Polyester tire.

Figure 5: Rubber sheet (the left sheet was used in this test).

2.2.2. Freeze-Thaw Processing.

The freeze-thaw conditioning process mainly simulated the effect of high- and low-temperature cycles on the aggregate in the natural environment. In the laboratory, the freeze–thaw cycles of the hard sandstone aggregate were performed as follows:

(1) The hard sandstone aggregate samples were placed in stainless steel basins and kept in an oven at 180°C for 24 h.

(2) The stainless steel basins with the aggregate were filled with water when the temperature of the aggregate was 180°C. At this temperature, large amounts of hot water vapor formed, as shown in Figure 9.

(3) The stainless steel basins with aggregates and water were kept in a refrigerator at −18°C for 24 h.

(4) After the stainless steel basins with aggregate had been frozen at −18°C for 24 h, they were placed in an oven at 180°C and dried to a constant weight.

(5) After (1)–(4), a freeze-thaw cycle was completed.

Figure 6: British pendulum tester.

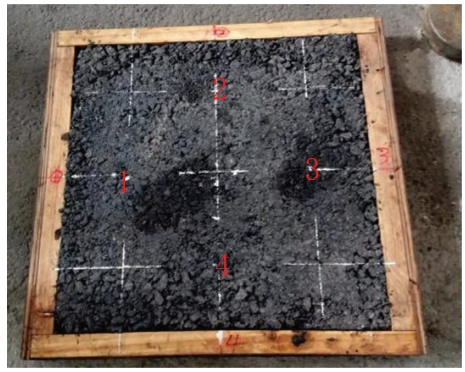

Figure 7: Test points of the British pendulum number measured with the British pendulum tester.

Figure 8: Heating and drying using natural gas combustion.

3. Composition of Hard Sandstone

The sandstone was identified as gravel-bearing coarse-grained tuffaceous sandstone with dark gray, gravel-bearing, sand-like, and sheet-like structures. It was composed of chlorite and was mainly felsic. The felsic substance was granular, with sizes between 0.01 and 0.1 mm. Sericite was in the form of colorless phosphorous flakes, and chlorite was in the form of green scales. Figure 10 shows an image of the hard sandstone under a polarized light microscope, and Table 2 shows the main mineral components.

4. Materials

4.1. Coarse Hard Sandstone Aggregate. First, the physical properties of the hard sandstone aggregate were measured using standard test methods [13], and Table 3 shows the results. Because the adhesion of the aggregate to asphalt has a direct effect on the water stability of HMA, the boiling water method [14] was used to evaluate the adhesion between the hard sandstone aggregate and the asphalt, as shown in Figure 11. The asphalt film on the hard sandstone aggregate surface was completely preserved, and the

Figure 9: Freeze and thaw cycles of the hard sandstone coarse aggregate.

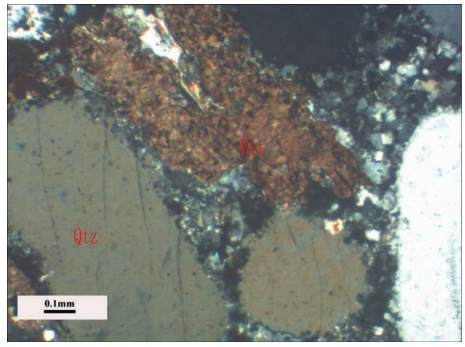

Figure 10: Image of sandstone under a polarized light microscope.

Table 2: Main mineral components of hard sandstone.

Mineral components	Gravel (%)	Sand chips (%)	Interstitial components (%)
Results	10	70	20

percentage of the stripping area was close to 0. Hence, the adhesion level between the hard sandstone aggregate and asphalt was 5.

4.2. Fine Aggregate. The fine aggregate was limestone-manufactured sand, and Table 4 shows its properties.

4.3. Filler. The filler was a limestone grinding powder, and Table 5 shows its properties.

4.4. Asphalt. Styrene-butadiene-styrene (SBS)-modified asphalt was used, and Table 6 shows its properties.

5. Results for Hard Sandstone Aggregate after Various Conditioning Treatments

To further study the effects of heating, drying, and high-temperature storage on the properties of the hard sandstone aggregate, the processes of heating, drying, storage, and rolling were simulated in the laboratory and then the crushing values, PSVs, and wear loss rates were measured.

5.1. Crushing Value

5.1.1. Effect of Storage Time on the Crushing Value. The hard sandstone aggregate samples were subjected to heating and drying using natural gas combustion. Subsequently, they

Table 3: Properties of the hard sandstone coarse aggregate measured using standard test methods.

Properties	Unit	Requirements	Results
Crushing value	%	≤26	23.4
Los Angeles abrasion	%	≤28	25.0
Polished stone value	BPN	≥42	56
Bulk relative density			
5–10 mm	—	≥2.60	2.715
10–15 mm			2.714
Water absorption			
5–10 mm	%	≤2.0	0.45
10–15 mm			0.43
Flat and elongated particles			
>9.5	%	≤12	11.1
<9.5		≤18	12.8
Particle content <0.075 mm (washing)	%	<1	0.9
Durability/soundness	%	≤12	6

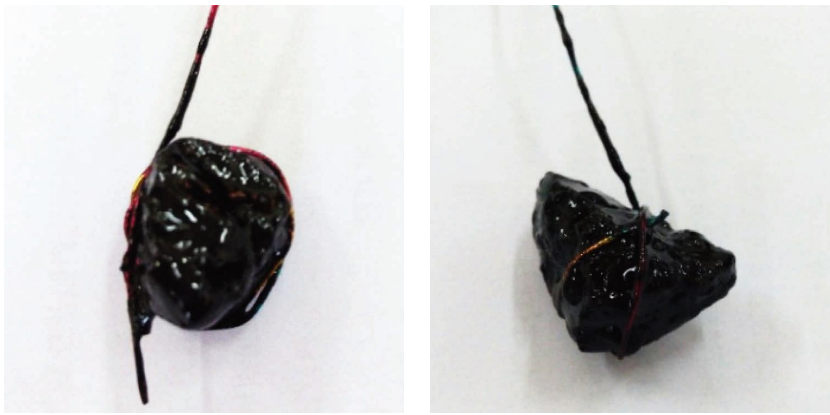

(a) (b)

Figure 11: Adhesion between the hard sandstone aggregate and asphalt. (a) #70 road petroleum asphalt and (b) styrene-butadiene-styrene (SBS) (I-D)-modified asphalt.

Table 4: Properties of fine aggregate.

Properties	Unit	Technical requirements	Results
Apparent relative density	—	≥2.50	2.62
Methylene blue value	g/kg	≤25	16
Angularity	s	≥30	45

Table 5: Properties of filler.

Properties	Unit	Technical requirements	Results
Apparent density	g/cm^3	≥2.50	2.679
Water content	%	≤1	0.3
Hydrophilic coefficient	—	<1	0.75
Particle size			
<0.6 mm	%	100	100
<0.15 mm	%	90–100	98.8
<0.075 mm	%	75–100	87.4

were placed in an oven and maintained at a temperature of 180°C for durations of 30, 60, and 120 min. Following this, the crushing values were determined at a temperature of 180°C. Figure 12 shows the values.

Figure 10 displays the crushing values of the hard sandstone aggregate under various conditions. The crushing values of the hard sandstone aggregate stored in a blast drying oven at 180°C for different durations after burning

Table 6: Properties of SBS-modified asphalt.

Properties	Unit	Technical requirements	Results
Penetration depth at 25°C, 100 g, 5 s	0.1 mm	40–60	50
Softening point (ring and ball method)	°C	≥60	85.0
Ductility at 5 cm/min, 5°C	cm	≥20	39
Specific relative density at 15°C	—	—	1.060
Rolling thin-film oven test at 163°C			
Weight change	%	±1.0	−0.105
Retained penetration	%	≥65	67
Ductility at 5°C	cm	≥15	19

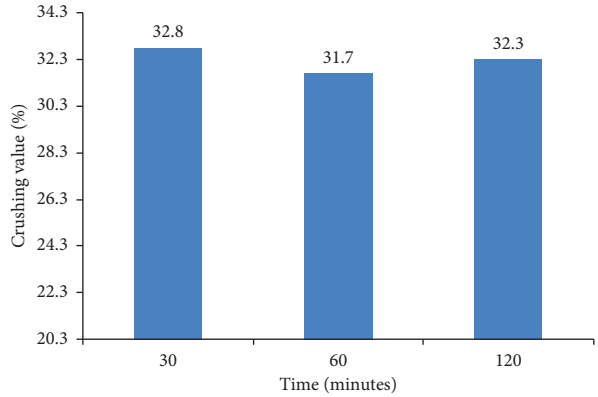

Figure 12: Aggregate crushing values after heating and storage at 180°C.

and drying with natural gas were as follows: 32.8% for 30 min, 31.7% for 60 min, and 32.3% for 120 min. To analyze the influence of the storage time at 180°C on the crushing value, a one-way analysis of variance (ANOVA) at the 95% confidence level ($\alpha = 0.05$) was used. Table 7 shows the results, and it was found that the P value was greater than 0.05, which fully indicates that the storage time at 180°C had no significant influence on the crushing value.

5.1.2. Effect of Temperature on the Crushing Value. During the initial compaction, recompaction, and final compaction stages for HMA, the temperature of the mixture was reduced by approximately 90°C from 180°C [19], which could lead to varying degrees of crushing of the hard sandstone aggregate. To replicate this phenomenon, the crushing values of the hard sandstone aggregate were assessed at 20°C, 140°C, 160°C, and 180°C. Figure 13 shows the results.

A crushing value of 23.4% was obtained at room temperature (20°C). Crushing values of 23.3% and 23.2% were obtained when the hard sandstone aggregate was only maintained for 2 h in an oven at constant temperatures of 140°C and 160°C, respectively. Furthermore, a higher crushing value of 32.3% was measured for the hard sandstone aggregate sample that was first heated using natural gas combustion and then placed in the oven at 180°C for 2 h.

According to Figure 11, the crushing values remained relatively consistent at temperatures of 20°C, 140°C, and 160°C. Based on the results of the one-way ANOVA of the crushing values at 20°C, 140°C, and 160°C, as shown in Table 8, the P value was larger than 0.05, which proved that the temperature had no significant effect on the crushing value when the temperature of the hard sandstone aggregate was 160°C and below. However, when the hard sandstone aggregate was first heated using natural gas combustion and then placed in the blast drying oven at 180°C for 2 h, its crushing value increased to 32.3%. This indicated that the burning and storage of the hard sandstone aggregate in the blast drying oven at 180°C for 2 h significantly affected its crushing value.

5.1.3. Effect of Freeze-Thaw Cycles on the Crushing Value. The crushing values of the hard sandstone aggregate were measured after being subjected to zero, one, three, and five freeze-thaw cycles. Figure 14 shows the influence of the number of freeze-thaw cycles on the crushing value of the hard sandstone aggregate. Overall, the freeze-thaw cycles had little influence on the crushing value. However, one-way ANOVA was performed for the data in Figure 7, and Table 9 shows the result. It was found that the P value was less than 0.05, which showed that the number of freeze-thaw cycles affected the crushing value.

5.2. Polished Stone Value. To assess the influence of the freeze-thaw cycles on the skid resistance of the hard sandstone aggregate, freeze-thaw cycle tests of the hard sandstone aggregate were conducted in the laboratory and

Table 7: One-way analysis of variance (ANOVA) on effects of storage time on the crushing value.

Source	SS	df	MS	F	P value	F crit
Treatment	2135.707	1	2135.707	2.033713	0.226992	7.708647
Error	4200.607	4	1050.152			
Total	6336.313	5				

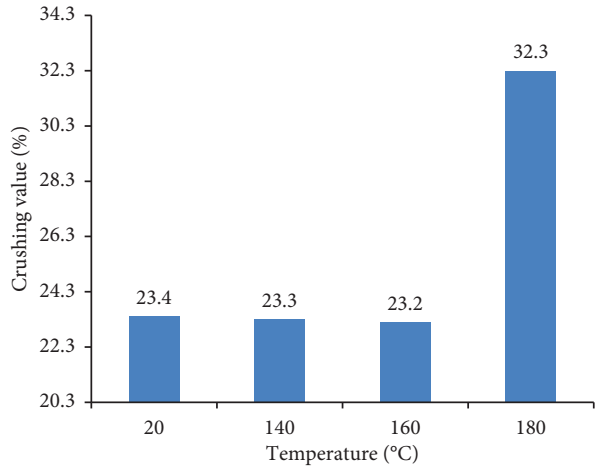

Figure 13: Crushing values at various temperatures.

Table 8: One-way ANOVA on effects of temperature at 160°C and below on the crushing value.

Source	SS	df	MS	F	P value	F crit
Treatment	10,425	1	10,425	3.636622	0.129193	7.708647
Error	11,466.69	4	2866.672			
Total	21,891.69	5				

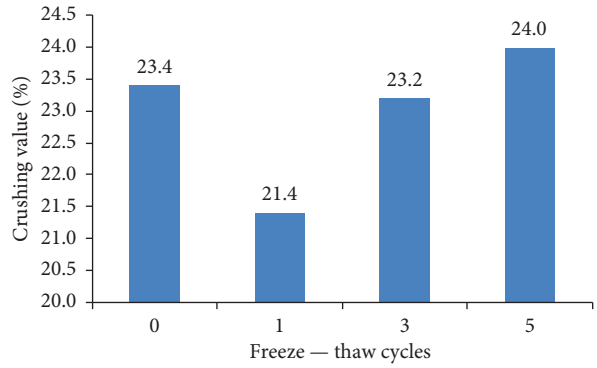

Figure 14: Crushing value vs. the number of freeze-thaw cycles.

Table 9: One-way ANOVA on effects of the number of freeze-thaw cycles on the crushing value.

Source	SS	df	MS	F	P value	F crit
Treatment	861.125	1	861.125	279.1329	2.94×10^{-6}	5.987378
Error	18.51	6	3.085			
Total	879.635	7				

then an accelerated polishing machine was used to accelerate the grinding of the hard sandstone aggregate. The PSVs were tested using a pendulum friction coefficient meter. Figure 15 shows the results.

Figure 15 illustrates the results obtained after zero, one, three, and five freeze-thaw cycles, indicating that the hard sandstone aggregate exhibited a minimum value of 56 and a maximum value of 60. Interestingly, these PSVs did not

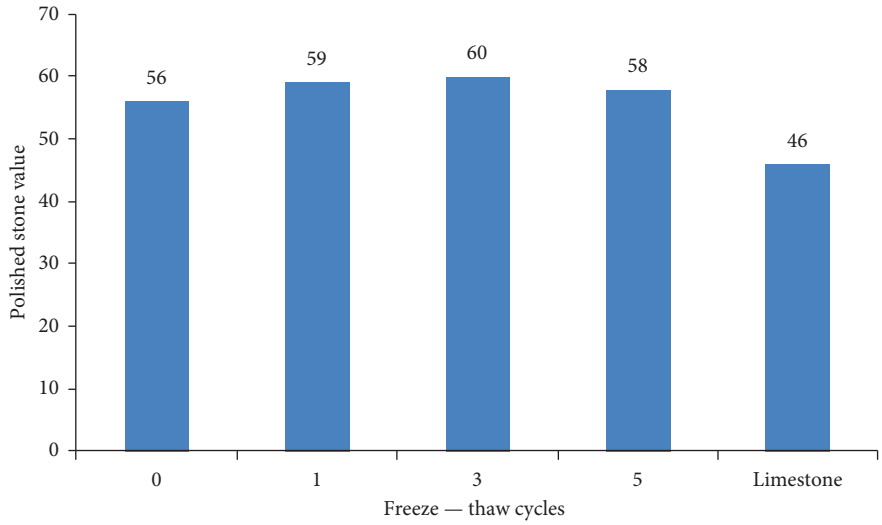

Figure 15: Polished stone value (PSV) vs. the number of freeze-thaw cycles.

exhibit a decrease as the number of cycles increased. After the freeze-thaw cycles, the PSVs of the hard sandstone aggregate were only slightly larger than that with no freeze-thaw cycles by 2–4 PSV units. However, it was found that the number of freeze-thaw cycles affected the PSVs with one-way ANOVA, as shown in Table 10. The PSVs of the hard sandstone aggregate were greater than those of aggregates such as limestone, diabase, and basalt shown in Table 1, which indicated that the hard sandstone aggregate had a better wear resistance.

5.3. Los Angeles Abrasion Loss. After subjecting the hard sandstone aggregate to freeze-thaw cycles, Los Angeles abrasion tests were conducted using a Los Angeles machine. Figure 16 presents the test results. The Los Angeles abrasion values of the hard sandstone aggregate increased after one freeze-thaw cycle, but after three and five freeze-thaw cycles, the Los Angeles abrasion values hardly changed compared with that after one freeze-thaw cycle. The one-way ANOVA results shown in Table 11 revealed that the number of freeze-thaw cycles had a significant influence on the Los Angeles abrasion values.

6. Surface Free Energy of Hard Sandstone Aggregate

To assess the adhesion between the hard sandstone aggregate and the asphalt, the surface free energy was measured using the CRM [15]. Table 12 presents the results. In addition, the surface energy for the limestone aggregate was measured, and the results indicated that the limestone aggregate had good adhesion properties to asphalt [17]. Table 12 also presents the results of the surface energy measurements obtained by Yi et al. [16] using atomic force microscopy. Their findings revealed that the surface energy of sandstone was higher than that of limestone.

The total surface free energy of hard sandstone shown in Table 12 was slightly greater than that of limestone. This could be attributed to the coarser surface of the hard sandstone compared with that of limestone [18]. Consequently, hard sandstone demonstrated a remarkable ability to withstand moisture damage when used as an aggregate in asphalt mixtures.

7. Effect of Marshall Compaction on the Impact Value of the Hard Sandstone Aggregate

During the compaction process for HMA, road rollers can crush the aggregate, resulting in a change in the aggregate grading curve of the asphalt mixture. Therefore, in the laboratory, we conducted a series of tests to investigate this phenomenon. To begin, we compacted the hard sandstone AC-13C with an asphalt-aggregate ratio of 4.6% using the Marshall compactor. This involved subjecting the sample to 75 blows on both sides. Subsequently, we performed extraction and screening tests [14] to determine the passing percentage of each grade of aggregate. Table 13 shows the results of these tests.

According to the data presented in Table 13, the standard Marshall compactor was used to compact the AC-13C asphalt mixture consisting of the hard sandstone aggregate. The passing percentage of aggregate particles in the size range of 4.75–16.0 mm remained relatively stable after the compaction process. Furthermore, it was found that the passing percentage of aggregate particles larger than 4.75 mm fell within the acceptable range of ±6%, as specified in the gradation requirements [19]. This indicated that the hard sandstone aggregate could withstand compaction with the Marshall compactor.

8. Moisture Susceptibility of Hard Sandstone AC-13C

There are many highway performance characteristics for HMA, such as rutting, low-temperature cracking, fatigue, and moisture susceptibility. Aggregate properties are one of the main factors affecting the moisture stability of HMA. Hence, the moisture susceptibility of AC-13C containing

Table 10: One-way ANOVA on effects of the number of freeze-thaw cycles on the PSVs.

Source	SS	df	MS	F	P value	F crit
Treatment	6272	1	6272	1601.362	1.63×10^{-8}	5.987378
Error	23.5	6	3.916667			
Total	6295.5	7				

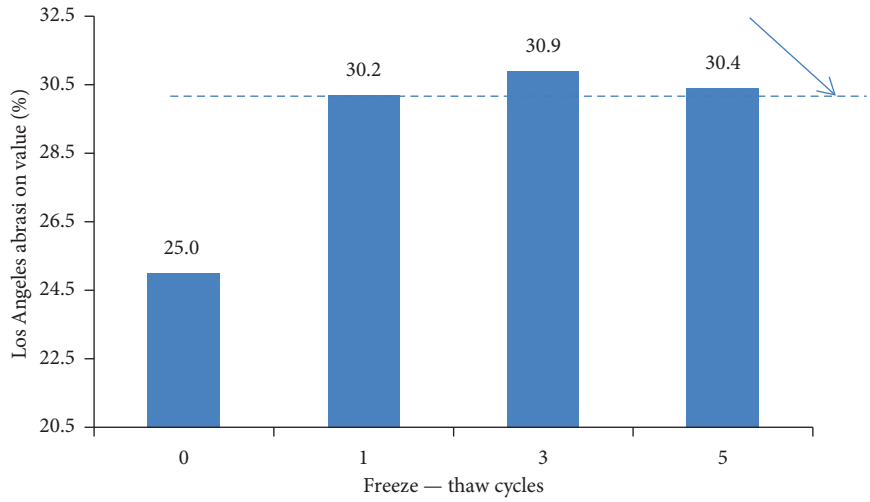

Figure 16: Abrasion value vs. the number of freeze-thaw cycles.

Table 11: One-way ANOVA results on effects of the number of freeze-thaw cycles on the Los Angeles abrasion values.

Source	SS	df	MS	F	P value	F crit
Treatment	1444.531	1	1444.531	229.9141	5.19×10^{-6}	5.987378
Error	37.6975	6	6.282917			
Total	1482.229	7				

Table 12: Surface free energy of hard sandstone aggregate and limestone aggregate (mJ/m^2).

Type of aggregate	Limestone	Hard sandstone	Limestone [16]	Sandstone [16]
Surface energy	56.48	60.01	64.99	68.33

Table 13: Results of extracting AC-13C of the hard sandstone aggregate (passing percentage).

Sieve size (mm)	16	13.2	9.5	4.75	2.36	1.18	0.6	0.3	0.15	0.075
Origin gradation	100	95	76	50	34	24	16	11	8	5
Results	100	96.6	76.9	44.4	33.5	27.1	22.6	17.0	13.1	8.4
Difference	0.0	1.6	0.9	−5.6	−0.5	3.1	6.6	6.0	5.1	3.4

hard sandstone aggregate was investigated. First, the optimum aggregate-asphalt ratio of AC-13C was obtained with the Marshall mix design method. Then, the moisture susceptibility of the hard sandstone AC-13C was tested with freeze-thaw cycle indirect tensile tests and simple performance tests.

8.1. Optimum Aggregate-Asphalt Ratio. Through aggregate sieve analysis, the combined aggregate gradation of the AC-13C asphalt mixture was designed, as shown in Figure 17. By using the Marshall mix design method [11], Figure 18 shows the curves relating the bulk specific gravity, Marshall stability (MS), flow value (FL), air void content (AV), voids in mineral aggregate (VMA), and voids filled with asphalt (VFA) to the asphalt-aggregate ratio.

Second, the four asphalt-aggregate ratios selected above were averaged as follows:

Based on the results in Figure 18, firrst, the following optimum asphalt-aggregate ratios were determined: (a) asphalt-aggregate ratio at maximum bulk specific density, a_1; (b) asphalt-aggregate ratio at maximum MS, a_2; (c) asphalt-

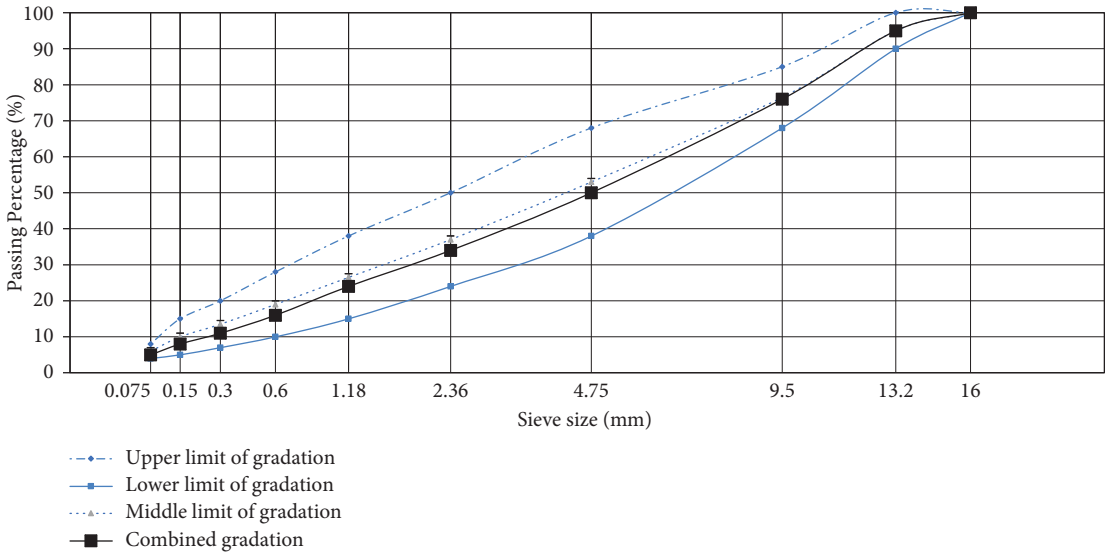

Figure 17: Aggregate combined gradation curve.

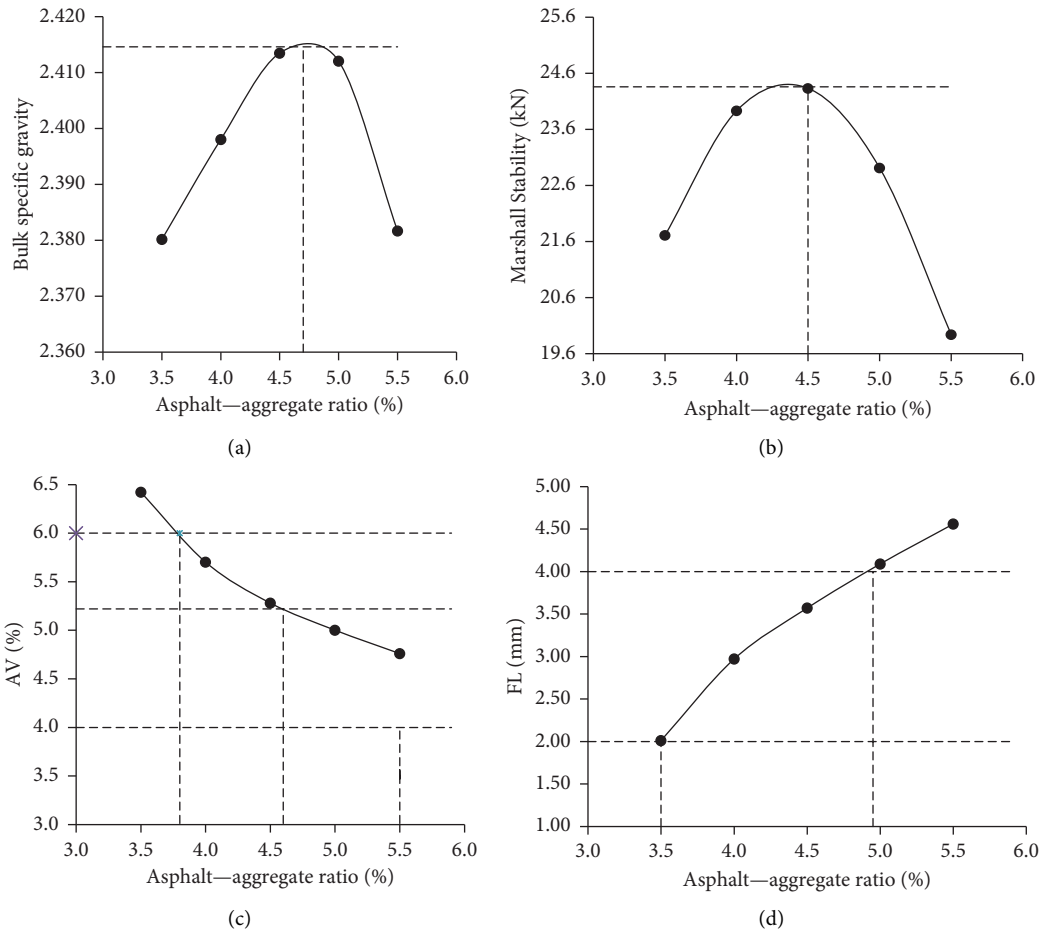

Figure 18: Continued.

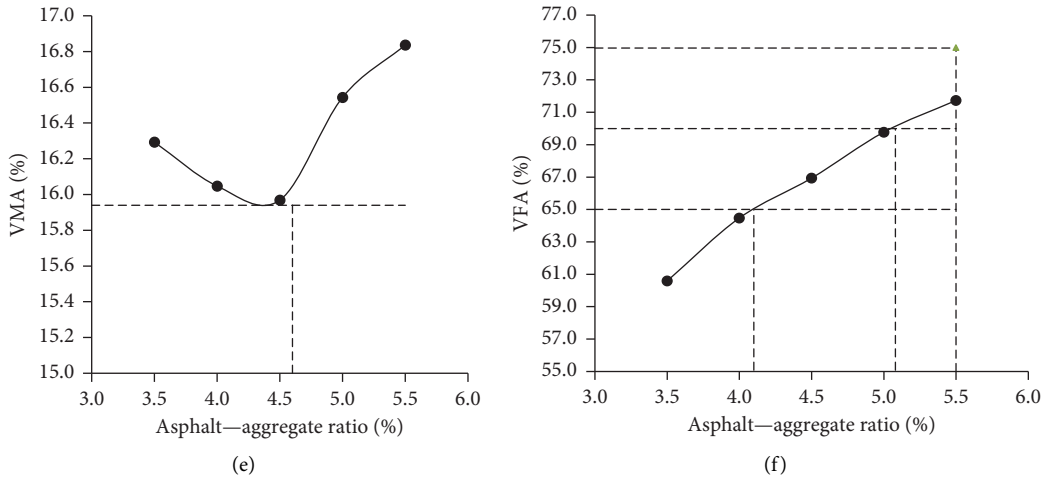

Figure 18: Design graphs for the Marshall mix design. (a) Bulk specific gravity. (b) Marshall stability. (c) Air void content. (d) Flow value. (e) Voids in mineral aggregate. (f) Voids filled with asphalt.

aggregate ratio at mid-point of specified AV range (4–6%), a_3; and (d) asphalt-aggregate ratio at mid-point of specified VFA range (65–75%), a_4.

$$OAC_1 = \frac{(a_1 + a_2 + a_3 + a_4)}{4} = \frac{(4.7\% + 4.5\% + 5.0\% + 5.1\%)}{4} = 4.83\%. \quad (4)$$

Third, the ranges of the asphalt-aggregate ratio, OAC_{min}-OAC_{max}, that meet the technical specifications (excluding VMA) were determined and averaged as follows:

$$OAC_2 = \frac{(OAC_{min} + OAC_{max})}{2} = \frac{(3.8\% + 5.0\%)}{2} = 4.40\%. \quad (5)$$

Fourth, OAC_1 and OAC_2 were averaged as follows:

$$OAC = \frac{(OAC_1 + OAC_2)}{2} = \frac{(4.83\% + 4.40\%)}{2} = 4.6\%. \quad (6)$$

The optimum asphalt-aggregate ratio was 4.6%.

8.2. Moisture Stability Test of AC-13C with Hard Sandstone. When an asphalt mixture pavement is subjected to water-temperature-load multifield coupling, its strength and modulus will decay and various diseases will appear in the asphalt mixture pavement, such as cracking and raveling.

8.2.1. Freeze-Thaw Indirect Tensile Test. The immersion Marshall test and freeze-thaw indirect tensile test are commonly conducted to evaluate the water stability of asphalt mixtures. The standard Marshall specimens were prepared by double-sided compaction 50 times in the laboratory, and based on a vacuum saturation and freeze-thaw process, the indirect TSR of the hard sandstone AC-13C was determined to be 81.2%, which exceeded the corresponding technical requirements of 80%.

8.2.2. Simple Performance Test. To further evaluate the water stability of the hard sandstone AC-13C, the dynamic modulus was measured with the simple performance test, and the water stability was evaluated by the residual dynamic MR [21–24]. First, hard sandstone AC-13C samples were subjected to the vacuum saturation and freeze-thaw process and then the dynamic moduli were measured. Table 14 shows the dynamic moduli of the freeze-thaw and non-freeze-thaw cycle groups.

From the results in Table 10, it was found that the dynamic modulus of the hard sandstone AC-13C decreased to 71–76% after one freeze-thaw cycle as the frequency increased. Based on the dynamic MR of 60% recommended by Jason Bausano et al. [24], the hard sandstone AC-13C had a good water-resistance ability. At the same time, the phase angle increased after one freeze-thaw cycle, as shown in Table 15.

From the results in Table 11, it was found that the phase angle increased by 5–10% as the frequency decreased, so the viscous component of the hard sandstone AC-13C increased, and the elastic component was reduced. Figure 19 shows the main curve of the hard sandstone AC-13C after one freeze-thaw cycle. The main curve of the freeze-thaw groups was below the main curve of the nonfreeze-thaw groups over the entire frequency range, and as the frequency increased, the difference in the dynamic moduli between the two was greater. Therefore,

Table 14: Dynamic modulus of the hard sandstone asphalt mixture AC-13C at 20°C.

Frequency (Hz)	Non-freeze-thaw groups (MPa)	Freeze-thaw groups (MPa)	Percentage (%)
10	7961.7	6058.7	76.1
1.0	4514.3	3333.0	73.8
0.1	2199.0	1567.3	71.3

Table 15: Phase angle of the hard sandstone asphalt mixture AC-13C at 20°C.

Frequency (Hz)	Non-freeze-thaw groups (MPa)	Freeze-thaw groups (MPa)	Percentage (%)
10	21.1	22.3	105.7
1.0	26.2	28.1	107.3
0.1	29.4	32.4	110.5

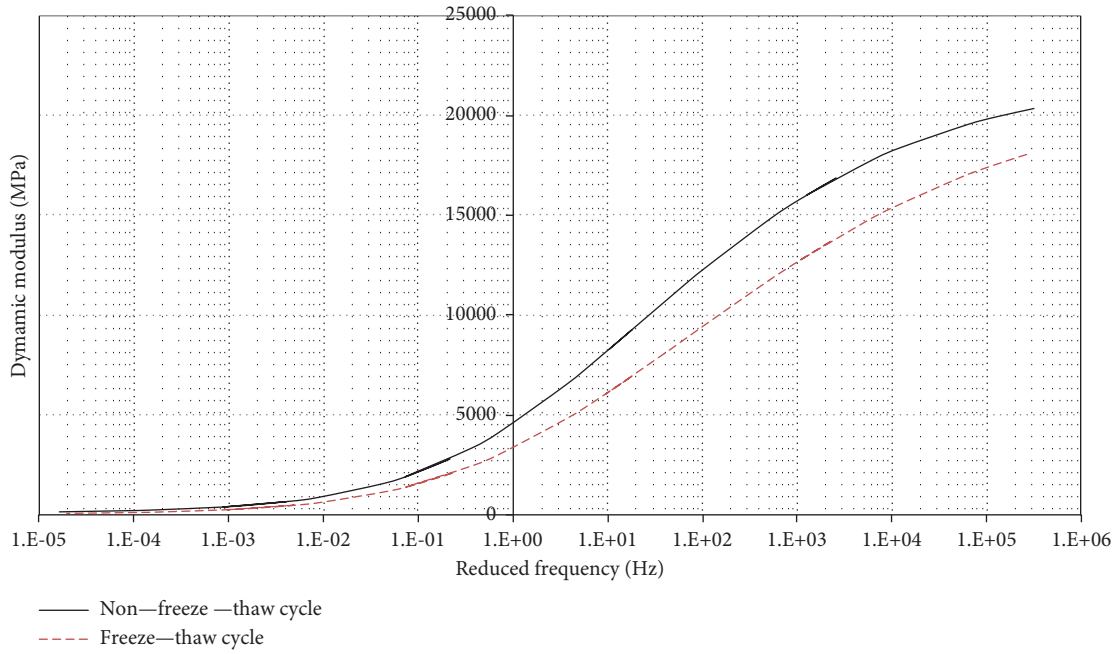

Figure 19: Curves of the hard sandstone AC-13C.

after one freeze-thaw cycle, the hard sandstone AC-13C was damaged inside, and the dynamic modulus became small, which fully showed that the asphalt pavement was damaged by water.

9. Three-Wheel Polishing Test for Hard Sandstone AC-13C

A hard sandstone AC-13C sample with dimensions of 50 cm × 50 cm × 5 cm was made in the laboratory. The AV was carefully maintained at 5.2% after compaction. Figure 20 shows the forming process.

As shown in Figure 21, the British pendulum number of the hard sandstone AC-13C sample gradually decreased with the number of polishing cycles. At the end of 160,000 three-wheel polishing device (TWPD) cycles, the British pendulum number was approximately 58, which was close to the PSV of the hard sandstone aggregate shown in Figure 15.

After 160,000 TWPD cycles, there was a ring wheel track on the sample, and it was found that some aggregate particles had white spots on their surfaces, indicating that the asphalt film fell off and that the aggregate was gradually polished, as shown in Figure 22.

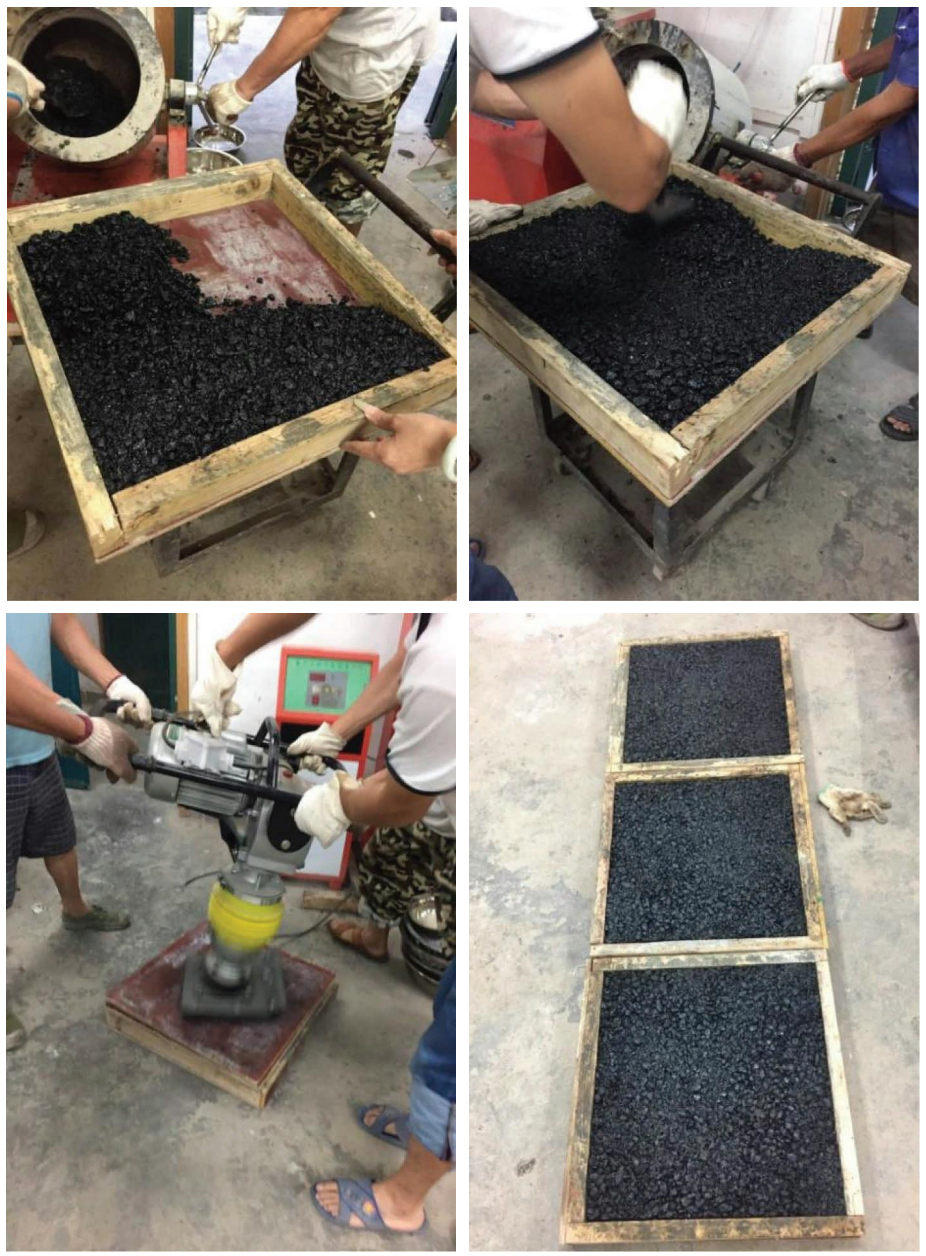

Figure 20: Forming process of the hard sandstone AC-13C.

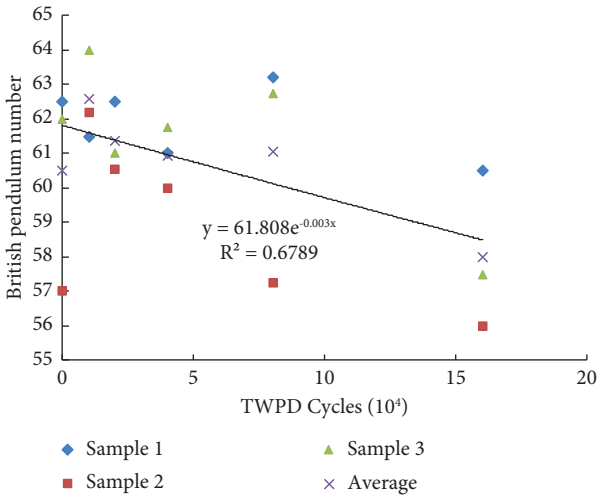

Figure 21: British pendulum number vs. three-wheel polishing device (TWPD) cycles.

Figure 22: Three-wheel polishing test of the hard sandstone AC-13C.

10. Conclusions

In this study, the hard sandstone aggregate was conditioned by heating, drying, high-temperature storage, and freeze-thaw cycles, and its properties were tested by aggregate crushing, accelerated polishing, and Los Angeles abrasion tests. The moisture susceptibility of HMA containing the hard sandstone aggregate was evaluated with the indirect TSR and the MR, and the polishing test of HMA containing the hard sandstone aggregate was conducted with the three-wheel polishing tester.

The results proved that it is feasible to use hard sandstone aggregate in HMA. The main conclusions are as follows:

(1) The aggregate crushing value was almost unaffected by the storage time at high temperatures.

(2) The temperature had no significant effect on the crushing value when the temperature of the hard sandstone aggregate was 160°C and below. The combined action of natural gas combustion drying and storage at 180°C had a significant influence on the crushing value of the hard sandstone aggregate.

(3) The number of freeze-thaw cycles affected the crushing value.

(4) The number of freeze-thaw cycles affected the PSV, as shown by one-way ANOVA.

(5) After three and five freeze-thaw cycles, the Los Angeles abrasion values hardly changed compared with that after one freeze-thaw cycle, but the number of freeze-thaw cycles had a significant influence on the Los Angeles abrasion values based on one-way ANOVA.

(6) The hard sandstone had a high surface free energy.

(7) Through the Marshall compaction test, the combined aggregate gradation curve of the AC-13C asphalt mixture changed little, which met the corresponding technical requirements.

(8) The hard sandstone AC-13C had a good anti-moisture susceptibility with the TSR and the MR.

(9) At the end of 160,000 cycles, the British pendulum number of the hard sandstone aggregate was approximately 57, as determined using a three-wheel polishing tester.

(10) Methodological limitations were as follows:

In the laboratory, the hard sandstone aggregates were first heated and dried using natural gas combustion for 30 min, which is different from the heating and drying methods used in batch HMA facilities. In batch HMA facilities, the aggregate is heated and dried in a rotating state. In the laboratory, the aggregate is heated and manually stirred for drying, which may cause uneven heating and drying of the aggregate, thus affecting the test results. In the laboratory, through freeze-thaw cycles, the aggregate was subjected to temperature and humidity in a way that is different from the temperature and humidity in asphalt pavement, which may have affected the test results. The shortcomings of the above methods will be further improved and perfected in the future work.

Data Availability

The authors declare that all the data in this manuscript were obtained through experiments and are correctly presented. The data used to support the findings of this study are included within the article.

Conflicts of Interest

The authors declare that they have no conflicts of interest to report regarding the present study. The manuscript was approved by all authors for publication. The authors declare that the work described in this manuscript is original research and has not been publicly published previously.

Authors' Contributions

The work presented herein was performed in collaboration among all the authors. LP was responsible for the study conception and design. YL was responsible for data collection and project application. HJ and LY were also responsible for data collection. YD was responsible for the writing and refinement of the paper and is the corresponding author. All the authors reviewed the results and approved the final version of the manuscript.

Acknowledgments

This study was funded by the "Research on the Application of Granite Aggregates on the Highway from Guilin to Qinzhou Port (Nanning Liujing to Binyang section) in Guangxi (LBGS-HT-51)" and the "Research on the Application of Guangxi Granite Asphalt Concrete in Highway Pavement Engineering" from the Department of Science and Technology of the Guangxi Zhuang Autonomous Region (1598009-11), and "Study on Two lift (wet-on-wet) concrete composite pavement" from the Department of Science and Technology of the Guangxi Zhuang Autonomous Region (Guike AB20159036).

References

[1] X. Ouyang, C. Zhao, P. Gao, and X. Wang, "Analysis of influencing factors of performance for sandstone asphalt mixture," *IOP Conference Series: Earth and Environmental Science*, vol. 455, no. 1, Article ID 12088, 2020.

[2] C. H. A. R. L. E. S. T. Metcalf and W. H. Goetz, "Bituminous sandstone mixtures," 2023, https://docs.lib.purdue.edu/cgi/viewcontent.cgi?article=2573&context=roadschool.

[3] D. Q. Hunsucker and R. C. Graves, "Performance evaluations of crushed sandstone aggregates in bituminous bases," *Kentucky Transportation Center Research Report*, vol. 504, 1990.

[4] H. Zhang and H. Li, "Optimization of sandstone concrete pavement materials based on finite element method," *Arabian Journal for Science and Engineering*, vol. 46, no. 11, Article ID 10835, 2021.

[5] H. Li, X. Guo, J. Xin et al., "Study on the characteristics of sandstone and feasibility to replace limestone in cement stabilized macadam base," *International Journal of Pavement Research and Technology*, vol. 16, no. 6, pp. 1419–1438, 2023.

[6] M. Yılmaz and A. Tugrul, "The effects of different sandstone aggregates on concrete strength," *Construction and Building Materials*, vol. 35, no. 35, pp. 294–303, 2012.

[7] F. Yang, H. Li, G. Zhao, P. Guo, and W. Li, "Mechanical performance and durability evaluation of sandstone concrete," *Advances in Materials Science and Engineering*, vol. 2020, Article ID 2417496, 10 pages, 2020.

[8] A. Topal and P. A. Dokandari, "Laboratory comparison of aging characteristics of warm mix asphalts involving natural and synthetic water containing additives," *Materials Research*, vol. 17, no. 5, pp. 1129–1136, 2014.

[9] Fu Wang, H. Zhu, B. Shu et al., "Microwave heating mechanism and self-healing performance of asphalt mixture with basalt and limestone aggregates," *Construction and Building Materials*, vol. 342, Article ID 127973, 2022.

[10] H. Liu, Z. Wang, C. Yang et al., "Effect of coarse aggregate characteristics on skid resistance deterioration of the ultrathin wearing course," *Journal of Materials in Civil Engineering*, vol. 33, no. 4, Article ID 4021051, 2021.

[11] M. Sun, Bo Li, Z. Yi, K. Cao, A. Li, and Y. Wang, "Optimization of surface free energy parameters for asphalt binder-aggregate system based on RBF neural network model," *Construction and Building Materials*, vol. 357, Article ID 129382, 2022.

[12] S. Yi-Jun, Y. Wan-Hong, and D. Hui, "Research on aggregate crushing value based on different temperature," *Highway Transportation Science and Technology (Applied Technology Edition)*, vol. 12, no. 1, pp. 172-173, 2016.

[13] Jtg, *Highway Engineering Aggregate Test Regulations*, Ministry of Communications of the People's Republic of China, Beijing, China, 2005.

[14] Jtg, *Standard Test Methods of Bitumen and Bituminous Mixtures for Highway Engineering*, Ministry of Communications of the People's Republic of China, Beijing, China, 2011.

[15] D. Sinkonde, H. P. Wen, and X. Q. Yi, "Evaluate the simple surface energy of aggregates using the capillary rise method," *Journal of Testing and Evaluation*, vol. 35, no. 6, pp. 618–623, 2007.

[16] J. Yi, X. Pang, D. Feng et al., "Studies on surface energy of asphalt and aggregate at different scales and bonding property of asphalt–aggregate system," *Road Materials and Pavement Design*, vol. 19, no. 5, pp. 1102–1125, 2018.

[17] S. Cui, B. R. K. Blackman, A. J. Kinloch, and A. C. Taylor, "Durability of asphalt mixtures: effect of aggregate type and adhesion promoters," *International Journal of Adhesion and Adhesives*, vol. 54, pp. 100–111, 2014.

[18] Y. Gao, X. Liu, S. Ren, Y. Li, and Y. Zhang, "Role of surface roughness in surface energy calculation of aggregate minerals," *Transportation Research Record Journal of the Transportation Research Board*, vol. 2678, no. 1, pp. 190–201, 2023.

[19] Jtg, *Technical Specifications for Construction of Highway Asphalt Pavements*, Ministry of Communications of the People's Republic of China, Beijing, China, 2005.

[20] American Association of State Highway and Transportation Officials, *Standard Method of Test for Resistance of Compacted Asphalt Mixtures to Moisture-Induced Damage*, AASHTO, Washington DC, USA, 2003.

[21] A. Vargas-Nordcbeck, F. Leiva-Villacorta, J. P. Aguiar-Moya, and L. Loria-Salazar, "Evaluating moisture susceptibility of asphalt concrete mixtures through simple performance tests," *Transportation Research Record: Journal of the Transportation Research Board*, vol. 2575, no. 1, pp. 70–78, 2016.

[22] A. A. Nadkarni, K. E. Kaloush, W. A. Zeiada, and K. P. Biligiri, "Using dynamic modulus test to evaluate moisture susceptibility of asphalt mixtures," *Transportation Research Record: Journal of the Transportation Research Board*, vol. 2127, no. 1, pp. 29–35, 2009.

[23] J. Lee, S.-Je Moon, J. Im, and S. Yang, "Evaluation of moisture susceptibility of asphalt mixtures using dynamic modulus," *Journal of Testing and Evaluation*, vol. 45, no. 4, pp. 1280–1288, 2017.

[24] J. Bausano and R. C. Williams, "Transitioning from AASHTO T283 to the simple performance test using moisture conditioning," *Journal of Materials in Civil Engineering*, vol. 21, no. 2, pp. 73–82, 2009.
[25] T. W. Vollor and D. I. Hanson, "Development of laboratory procedure for measuring friction of HMA mixtures-PHASE I," NCAT Report 06-06, National Center for Asphalt Technology, Auburn, Alabama, 2006.
[26] S. Erukulla, "Refining a laboratory procedure to characterize change in hot-mix asphalt surface friction," Auburn, AL, USA, Master of Science Thesis.
[27] B. E. Marc Manuel Rached, *Use of Manufactured Sands for Concrete Paving*, University of Texas, Austin, TX, USA, 2011.